Noniterative Biexponential Fluorescence Lifetime Imaging in the Investigation of Cellular Metabolism by Means of NAD(P)H Autofluorescence

Raluca Niesner, Bülent Peker, Peter Schlüsche, and Karl-Heinz Gericke*[a]

The cofactors NADH and NADPH, hereafter NAD(P)H [NAD(P) = nicotinamide adenine dinucleotide (phosphate)], belong to the principal endogenous indicators of energetic cellular metabolism. Since the metabolic activity of cells is given by the ratio between the concentrations of free and protein-bound NAD(P)H, the development of autofluorescence techniques which accurately measure the modifications to this ratio is particularly significant. Hitherto the methods applied in the monitoring of cellular metabolism have provided either imprecise results, due to interference of the NAD(P)H signal by perturbing factors, or they have required a complicated internal calibration. We employ biexponential fluorescence lifetime imaging (FLIM) in order to discriminate between the free and protein-bound NAD(P)H without any previous calibration. Thus, we have obtained directly, and for the first time, a high-resolution map of cellular metabolism, that is, an image of the contribution of the protein-bound NAD(P)H to the cumulative NAD(P)H fluorescence signal. Moreover, we demonstrate that protein–NAD(P)H complexes characterised by different fluorescence lifetimes are not uniformly distributed all over the cell, as assumed until now, but are concentrated in certain cellular regions. The different fluorescence lifetimes indicate either different protein–NAD(P)H complexes or different bond strengths between NAD(P)H and the protein in these complexes.

Since an important aspect in biological applications is to monitor the dynamics of the relevant processes (such as cellular metabolism), rapid dynamical techniques, for example, rapid biexponential fluorescence lifetime imaging, are needed. Furthermore, it is necessary to reduce the evaluation effort as much as possible. Most of the evaluation techniques in multiexponential FLIM are time-expensive iterative methods. The few exceptions are connected with a loss of information, for example, global analysis; or a loss in accuracy, for example, the rapid evaluation technique (RLD). We implement for the first time in FLIM a noniterative, nonrestrictive method originally developed by Prony for approximations of multiexponential decays. The accuracy of this method is verified in biexponential FLIM experiments in time-domain on mixtures of two chromophores both in homogenous and in heterogeneous media. The resulting fluorescence lifetimes agree (within error margins) with the lifetimes of the pure substances determined in monoexponential FLIM experiments. The rapidity of our evaluation method as compared to iterative pixel-by-pixel methods is evidenced by a reduction of the evaluation time by more than one order of magnitude. Furthermore, the applicability of this method for the biosciences is demonstrated in the investigation of cellular metabolism by means of NAD(P)H endogenous fluorescence.

1. Introduction

Since a central aim of the biosciences is to simulate the real environmental conditions of biological systems in order to gain a true image of the processes of interest, the development of techniques which apply tissue autofluorescence, that is, nonlabelling techniques, is particularly important.[1–9] Endogenous chromophores which contribute to tissue intrinsic fluorescence are haemoglobin, reduced nicotinamide adenine dinucleotides (NADH and NADPH), oxidised flavoproteins, serotonin, collagen, elastin, etc.[1–9] As indicators of energetic metabolism, the cofactors NADH and NADPH, hereafter NAD(P)H [NAD(P) = nicotinamide adenine dinucleotide (phosphate)], are the principal topic of many research works.[1,4,5,7–11]

Despite the low two-photon absorption cross-section of most chromophores, two-photon microscopy (TPM) is adequate for studies which necessitate submicron, three-dimensional resolution, a large penetration depth in highly scattering media, and low photodamage of the sample outside the focal plane, that is, studies of biological systems.[7,8,12] In investigations of cellular NAD(P)H fluorescence, TPM has proven to have an additional advantage over the common confocal one-photon microscopy due to the reduced out-of-focus photobleaching effect.[8]

If the cofactors NADH and NADPH are employed as signal mediators, the cellular metabolic redox state is directly indicated by the ratio between the relative concentration of free NAD(P)H and of NAD(P)H involved in metabolic processes.[4,5,7,10,11] Consequently, the development of techniques which accurately measure variations in this ratio, that is, modifications of cellular metabolism, is particularly important.

[a] R. Niesner, B. Peker, P. Schlüsche, Prof. Dr. K.-H. Gericke
Institut für Physikalische und Theoretische Chemie
Technische Universität Braunschweig
Hans-Sommer Str. 10, 38106 Braunschweig (Germany)
Fax: (+49) 531-391-5396
E-mail: k.gericke@tu-braunschweig.de

One of the first and most common methods employed in the investigation of cellular metabolism is redox fluorimetry, in which the cumulative autofluorescence steady state signal of NAD(P)H (both free and protein-bound NAD(P)H) is registered.[4,5,8] Based on the different absorption and emission spectra of the two NAD(P)H states, the variations in the cumulative NAD(P)H signal are attributed to modifications to the concentration of free and protein-bound NAD(P)H and, thus, to modifications in the cellular redox state.[4,5] However, the signal registered is influenced not only by changes in NAD(P)H concentration, but also by other factors, such as light scattering, instrumental instability, sample movement or nonspecific background fluorescence originating from other biomolecules.[8] Thus, only qualitative, imprecise assertions about the metabolic cellular state can be inferred from redox fluorimetry studies.[8] Contrary to standard redox fluorimetry, in ratiometric redox fluorimetry the fluorescence signal of each species, that is (for example), of both free and protein-bound NAD(P)H, can be separately registered and analysed and, thus, an accurate assertion about the metabolic state can be made.[8] However, due to the complicated internal calibration of the set-up[8] and the ill-defined spectra[13] of the protein-bound NAD(P)H, ratiometric redox fluorimetry has never been used to investigate cellular metabolism by endogenous NAD(P)H fluorescence.

Fluorescence lifetime imaging (FLIM), which is based on the time-resolved registration of the fluorescence signal, is a versatile alternative to fluorimetric techniques.[13–15] The advantages of this method have been demonstrated both in labelling[16–20] as well as in nonlabelling experiments.[21–28] By employing FLIM, a very good contrast between the two NAD(P)H states can easily be obtained, since the fluorescence lifetimes of the free NAD(P)H (≈ 400 ps) and protein-bound NAD(P)H (≈ 2000 ps) differ significantly.[7,10,11]

In most FLIM experiments based on NAD(P)H autofluorescence, the registered cumulative fluorescence decay is approximated by a monoexponential function.[9–11] Thereby, a decrease in the resulting fluorescence lifetime indicates an increase in the free NAD(P)H concentration and, thus, a slower metabolic activity of the cells. However, this method has two major drawbacks. First, the cumulative NAD(P)H fluorescence decay deviates considerably from monoexponential behaviour—as we observed in our experiments—and, thus, a monoexponential approximation is inappropriate. Secondly, the changes in the fluorescence decay are caused not only by variations of free and protein-bound NAD(P)H concentrations but also by laser power fluctuations, light scattering and background noise.

Approximating the cumulative NAD(P)H fluorescence decay with a stretched exponential function solves only the first problem.[29] By employing biexponential FLIM, both disadvantages of monoexponential FLIM are counteracted: the cumulative NAD(P)H fluorescence decay is correctly approximated and the two NAD(P)H states are resolved so that the effect of interest, that is, modifications to the free and protein-bound NAD(P)H concentration, is separated from the effects of other perturbing factors. Although suggested by other authors,[9,10] to our knowledge biexponential NAD(P)H autofluorescence lifetime imaging has not been previously performed.

We performed biexponential FLIM combined with two-photon scanning microscopy in artificial skin constructs in order to study the cellular metabolism of dermal fibroblasts by means of NAD(P)H endogenous fluorescence. A typical result of such an experiment includes three images: the τ_1 map, that is, the fluorescence lifetime image of the free NAD(P)H, the τ_2 map, that is, the fluorescence lifetime image of the protein-bound NAD(P)H, and the ratio map, which mirrors the contribution of protein-bound NAD(P)H to the cumulative NAD(P)H fluorescence signal. Whereas the τ_1 map verifies the correctness of the experiment (the lifetime values should be ≈ 400 ps), the other two images reveal novel insight into cellular metabolism. As will be demonstrated later, the τ_2 map shows that different NAD(P)H–protein complexes characterised by different fluorescence lifetimes are not uniformly distributed all over the cell—as has always been assumed[9]—but are concentrated in certain cellular regions. The ratio map allows a direct and accurate monitoring of modifications to the free and protein-bound NAD(P)H content and, thus, of the cellular energetic state, as we verified in experiments in which the metabolic activity of fibroblasts under near infrared (NIR) photostress was probed.

An important aspect in the study of biological systems is to monitor the dynamics of the processes of interest, for example, cellular metabolism. However, due to the extreme evaluation effort, the performance of fast dynamical multiexponential FLIM experiments has failed until now.

Frequency-domain techniques and time-domain techniques, for example, time-correlated single-photon counting (TCSPC) and time-gated procedures, are principal methods of measuring the fluorescence decay time in an image.[13,30] In the frequency domain, the multiple-frequency FLIM (mfFLIM) associated with time-expensive, iterative, pixel-by-pixel Levenberg–Marquardt approximations was one of the first procedures employed to perform multiexponential FLIM.[23] A reduction in the evaluation effort was attained by means of global analysis techniques[24] combined with both mfFLIM and sfFLIM (single-frequency FLIM),[31] however, with the limitation of an invariant fluorescence lifetime all over the τ-image.

Evaluating the multiexponential FLIM in the time-domain is typically performed by means of time-expensive iterative methods, for example, nonlinear Marquardt methods.[25,26,29,32] An alternative noniterative, rapid evaluation technique (RLD) for mono- and biexponential decays was developed by Ashworth.[33–35] However, this method is restricted to a reduced number of data points (four for biexponential approximations),[35] which leads to imprecise results.[36] We performed biexponential FLIM experiments on homogenous mixtures of two dyes and determined their fluorescence lifetimes by means of RLD. The resulting lifetimes deviated constantly by more than 50% from the fluorescence lifetimes of the pure dyes measured in monoexponential FLIM experiments. Thus, RLD is not adequate as an evaluation method for biexponential FLIM and cannot be applied to multiexponential FLIM.

In order to achieve a rapid and accurate evaluation, we implemented (for the first time in FLIM) the numerical method originally developed by Prony for multiexponential nonitera-

tive approximations.[37,38] The accuracy of this method was verified in biexponential FLIM experiments in the time domain on mixtures of two substances both in homogenous as well as in heterogeneous media. The resulting fluorescence lifetimes generally deviate by less than 5% from the lifetimes of the pure substances determined in monoexponential FLIM experiments. The rapidity of our evaluation method as compared to iterative pixel-by-pixel methods is evidenced by a reduction in the evaluation time by more than one order of magnitude.

Multiexponential, noniterative approximation techniques similar to the Prony method have already been employed in the evaluation of fluorescence decays in nonimaging experiments.[39,40,41]

2. Noniterative Multiexponential FLIM Evaluation

The fluorescence intensity decay often deviates from the monoexponential behaviour, for example, the cumulative cellular NAD(P)H fluorescence decay. Thus, in order to resolve the components in a mixture by means of FLIM, it is favourable to approximate the time-dependent fluorescence intensity $F'(t)$ in each pixel by a multiexponential function, that is, with a sum of n exponential decays, as shown in Equation (1)

$$F'(t) = b + \sum_{i=1}^{n} a_i \cdot e^{-(t-t_{in})/\tau_i} + \varepsilon(t) \tag{1}$$

where b is the baseline, a_i are the prefactors of the exponential decays, τ_i are the corresponding lifetimes, t_{in} is the zero-point of the multiexponential decay, and $\varepsilon(t)$ is the noise of the experimental method. Since, under certain circumstances, the baseline b can be determined before the evaluation, the fluorescence signal becomes Equation (2).

$$F(t) = \sum_{i=1}^{n} a_i \cdot e^{-(t-t_{in})/\tau_i} + \varepsilon(t) \tag{2}$$

In our experiments, the averaged baseline b was measured by registering the signal of the sample immediately before the laser pulse.

A rapid and accurate modality for approximating the function $F(t)$ and, thus, for determining the fluorescence lifetimes τ_i and the corresponding prefactors a_i in the time domain is given by the method originally developed by Prony in order to distinguish between a biexponential and a triexponential function, which are almost identical in a small interval.[37,38] This method requires the data points (t_0,F_0), (t_1,F_1),…, (t_m,F_m) to be equidistant, whereby the time interval between two consecutive points is Δt.[37] Considering that $t_k = k \cdot \Delta t$, we can write Equation (3)

$$F_k = \sum_{i=1}^{n} \left(a_i \cdot e^{t_{in}/\tau_i} \right) \left(e^{-k \cdot \Delta t/\tau_i} \right) = \sum_{i=1}^{n} c_i \cdot \nu_i^k \tag{3}$$

for $k = 0,1,…, m$. Thus, for an n-exponential decay, we obtain a nonlinear set of m equations with $2n$ unknown variables, c_i and ν_i.[37]

To determine the variables ν_i, an nth-rank polynomial, Equation (4), with roots ν_i was used as an intermediate step[37]

$$\prod_{i=1}^{n} (\nu - \nu_i) = s_n + \sum_{i=1}^{n} s_{n-i} \cdot \nu^i = \varphi(\nu) \tag{4}$$

where s_i are the unknown prefactors of the nth-rank polynomial and $s_0 = 1$.

By multiplying all $\varphi(\nu_i)$ with the corresponding c_i and adding the resulting expressions, we obtain Equation (5).

$$\sum_{i=1}^{n} c_i \cdot \varphi(\nu_i) = F_n + \sum_{i=1}^{n} s_i \cdot F_{n-i} = 0 \tag{5}$$

This multiplication can be repeated with $c_i\nu_i$, $c_i\nu_i^2$,…, $c_i\nu_i^{m-n}$ and yields a set of $m-n+1$ equations with n unknown variables, s_i, Equation (6)[37]

$$\sum_{i=1}^{n} s_i \cdot F_{n+j-i} = -F_{n+j} \tag{6}$$

where $j = 0,1,…,m-n$. In this step, the unknown variables ν_i are transformed to the new variables s_i. If the condition $m-n+1 > n$ is satisfied, the upper set of equations is overdetermined and the unknown values s_i can be obtained by means of linear least-squares. By solving the polynomial equation $\varphi(\nu) = 0$, the values ν_i are determined. The equation $\varphi(\nu) = 0$ can be solved analytically up to the 4th order. Consequently, this method can be employed in all exponential evaluations, but it has a significant computational advantage over the usual iterative methods primarily in bi-, tri- and tetraexponential approximations.

Using the values ν_i, the lifetimes τ_i are given by Equation (7)

$$\tau_i = \frac{-\Delta t}{\ln(\nu_i)} \tag{7}$$

and Equation (3) becomes a linear set of m equations with only n unknown variables, c_i. By means of linear least-squares, Equation (3) can be solved and the values c_i calculated. Thus, the prefactors a_i are given by Equation (8).

$$a_i = c_i \cdot e^{-t_{in}/\tau_i} \tag{8}$$

The product $\tau_i \cdot a_i$ represents the integrated fluorescence signal of the individual species i, Equation (9)

$$\tau_i \cdot a_i = \int_0^{\infty} a_i \cdot e^{-t/\tau_i} dt \tag{9}$$

and it depends on: the concentrations C_i; the active one- and multiphoton absorption cross-sections $\phi_i\sigma_i$; the efficiencies η_i of the detection unit; the experimental calibration constant K; and on the excitation power P. Thereby, ϕ_i is the fluorescence

quantum yield and σ_i is the absolute one- and multiphoton absorption cross-section. Presuming that the detection efficiency η_i does not vary dramatically for different chromophores, the ratio $\tau_i \cdot a_i / \Sigma(\tau_i \cdot a_i)$, that is, the relative contribution of the component i to the cumulative fluorescence signal, is influenced by both the concentration C_i and by the active absorption cross-section $\phi_i\sigma_i$. Consequently, it is necessary to know the photophysical properties of the fluorescing species in order to calculate their relative concentration from the ratio $\tau_i \cdot a_i / \Sigma(\tau_i \cdot a_i)$.

A rather frequently observed deficiency of the Prony method is its significant sensitivity to experimental noise.[38] Therefore, Zhang et al. suggested an optimisation of the Prony method employed in the biexponential evaluation of single fluorescence decays (over 200 data points) by varying the acquisition time-window and by selecting other values for j in using Equation (6).[38] We tested the Prony method in our experiments, both in the genuine form and in the optimised form developed by Zhang. The results of the biexponential FLIM evaluation of 24 fluorescence intensity images registered at successive delays after the pulse, in steps of 200 ps, were the same (within error margins) by both methods and for the same computational effort. Moreover, the results agree with the fluorescence lifetimes of the components measured separately in monoexponential FLIM. Consequently, we chose to use the genuine Prony method to evaluate our FLIM experiments.

3. Results and Discussion

3.1. Validation of the Prony Method in Biexponential FLIM

In the following, the rapidity and accuracy of the Prony method as an evaluation technique in multiexponential fluorescence lifetime imaging is verified.

The evaluation of 24 consecutive fluorescence images (each $1.225 \cdot 10^5$ pixels) by means of the Prony method on a 1.7 GHz Celeron PC takes ≈ 20 s in our experiments, whereas the evaluation of $\approx 10^5$ pixels by iterative methods takes several minutes on a Sun workstation (pixel-by-pixel FLIM evaluation in frequency domain).[31] This comparison is evidence of the rapidity of our noniterative method which performs one loop per pixel, contrary to iterative methods which require eight to twenty-five iterations per pixel (pixel-by-pixel FLIM evaluation in time domain).[29] We also tested the accuracy of the Prony method in biexponential FLIM experiments on mixtures of two dyes, both in homogenous as well as heterogeneous media. The resulting fluorescence lifetimes were com-pared to the fluorescence lifetimes of the components measured separately in monoexponential FLIM experiments. Our results are in good agreement with the results of other authors who verified the Prony method in nonimaging fluorescence experiments.[38]

A first accuracy test in a homogenous medium was made on a mixture of 3,7-bis(diarylamino)-dibenzothiophen-S,S-dioxide (DBT 22) (45 μM) and rhodamine B (5 μM) in ethanol. Since the two-photon absorption cross-section $\phi\delta$, which reflects the fluorescing properties after two-photon excitation, is lower for DBT 22 ($1.22 \cdot 10^{-49}$ cm^{4}s) than for rhodamine B ($\approx 10^{-48}$ cm^{4}s), a mixture with a higher content of DBT 22 was used in the experiment, to avoid the signal of the less fluorescing component, that is, DBT 22, being masked by the background. The fluorescence lifetimes of the components, DBT 22 and rhodamine B, measured separately in monoexponential FLIM experiments, were 495 ps (FWHM = 60 ps) and 2587 ps (FWHM = 100 ps). For the ratio of their fluorescence lifetimes ($\tau_2/\tau_1 = 5.23$), the separation of the components by means of the Prony method can be performed optimally.[38] The full width at half maximum (FWHM) of the fluorescence lifetime distribution was influenced by the jitter of the detection unit, by fluctuations of the laser power and by other experimental factors. However, the centre of this distribution was determined with a precision of less than 1 ps.

In biexponential FLIM experiments on the aforementioned mixture, we determined, by means of the Prony method, a fluorescence lifetime of 472 ps (FWHM = 74 ps) for DBT 22 (τ_1) and 2608 ps (FWHM = 112 ps) for rhodamine B (τ_2, Figure 1). These values agree, within error margins, with the fluorescence lifetimes measured in monoexponential FLIM experiments. The separation between DBT 22 and rhodamine B was successful in 99.9% of the pixels. In the remaining 0.1% of the pixels, the fluorescence intensity was so low that the biexponential fluorescence decay was significantly disturbed by the experimental noise and the resulting fluorescence lifetimes corresponded
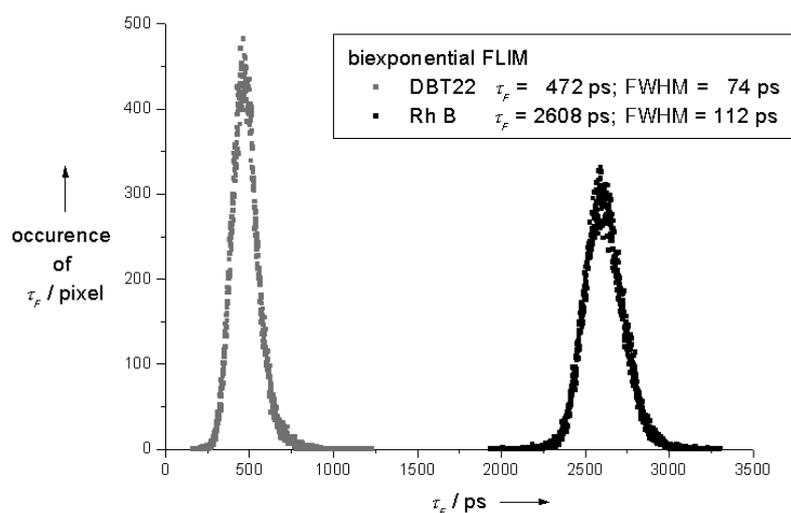

Figure 1. *Distribution of the fluorescence lifetime values of DBT 22 and of rhodamine B after the evaluation of the fluorescence decay images (biexponential FLIM) of a mixture of DBT 22 (45 μM) and rhodamine B (5 μM) in ethanol by means of the genuine Prony method.*

neither to DBT 22 nor to rhodamine B. The relative contribution ($\tau_2 a_2/(\tau_1 \cdot a_1 + \tau_2 \cdot a_2)$) of rhodamine B to the cumulative fluorescence signal amounted to 70.7%. The remaining 29.3% represents the relative contribution of DBT 22. These results qualitatively agree with the expected ratio ($\tau_2 a_2/(\tau_1 \cdot a_1 + \tau_2 \cdot a_2)$).

The parameters employed in this experiment were a scanned surface of 25×25 μm^2, a laser energy E_{pix} at the sample of 0.076 pJ/pixel, an excitation wavelength of 780 nm and an acquisition time of 3 s/frame. 24 fluorescence intensity images were depicted at subsequent delays after the laser pulse, in steps of 200 ps.

The fluorescence lifetimes of β-NADPH and rhodamine B in water (see Table 1), measured in monoexponential FLIM experiments, are 412 ps (FWHM = 15 ps) and 1530 ps (FWHM = 47 ps). An evaluation of the cumulative fluorescence decay of a mixture of β-NADPH (45 μм) and rhodamine B (5 μм) in distilled water registered in a biexponential FLIM experiment yielded a lifetime of 399 ps (FWHM = 175 ps) attributed to β-NADPH, and a lifetime of 1504 ps (FWHM = 147 ps) attributed to rhodamine B. The contribution of rhodamine B to the cumulative fluorescence signal amounted to 98.1% and that of β-NADPH was 1.9%. The experimental conditions were similar to those described above. This experiment is evidence that, by means of the Prony method, two fluorescing components can be accurately resolved, even if the lifetime ratio τ_2/τ_1 is rather low (3.7)[38] and the contribution of one component to the cumulative fluorescence signal is very large (98%).

The good separation of two chromophores from homogenous mixtures demonstrates that the Prony method is able to approximate biexponential fluorescence intensity decays correctly and creates a solid base for multiexponential FLIM in highly scattering heterogeneous media, for example, artificial skin constructs. In heterogeneous media, the experimental noise is amplified by the scattered light, which makes the separation of the components in a mixture by means of multiexponential FLIM difficult.

To demonstrate that the Prony method is able to approximate the cumulative fluorescence decay measured in biexponential FLIM experiments correctly, even under extreme conditions, we resolved trans-4-[4-(dimethylamino)-styryl]-1-methyl-pyridinium iodide (DASPI) and rhodamine B, two substances with very different fluorescing properties, in the double-stained epidermis ($\approx$ 7 μm depth) of artificial skin constructs (ASC), Figure 2. Figure 2a shows the steady-state intensity image of a
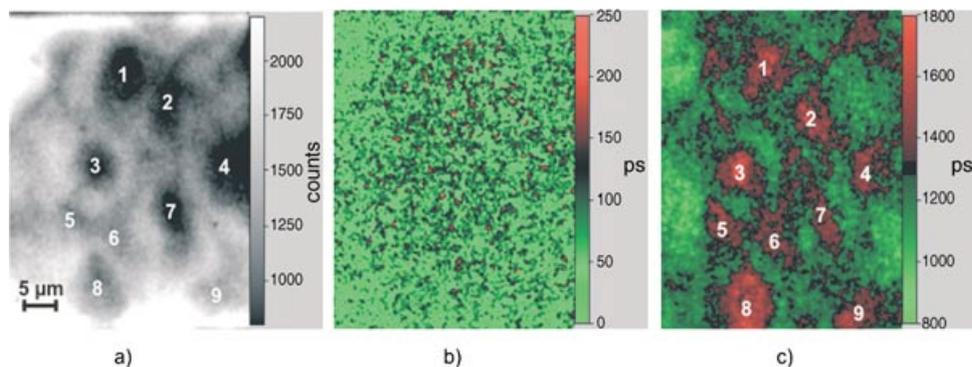

Figure 2. a) Intensity image of the artificial epidermis stained with a mixture of rhodamine B and DASPI, $\approx$ 7 μm in depth, b) τ_1 map corresponding to DASPI, c) τ_2 map corresponding to rhodamine B. The numbers in images (a) and (c) indicate nine different keratinocytes.

region containing nine keratinocytes in the artificial epidermis, and Figures 2b and c represent the fluorescence lifetime maps of DASPI and rhodamine B, respectively, of the same region. The resulting fluorescence lifetimes for DASPI and rhodamine B are 68 ps (FWHM = 40 ps) and 1377 ps (FWHM = 216 ps) respectively, which roughly corresponds to the values of their lifetimes in water measured in monoexponential FLIM experiments [DASPI: 61 ps (FWHM = 9 ps) and rhodamine B: 1530 ps (FWHM = 92 ps)]. The differences between the fluorescence lifetimes measured in water and those determined in the ASC are ascribed to environmental factors, for example, refractive index or viscosity.

In the τ_1 map attributed to DASPI, no structural differences between the cell interior and the lipidlike intercellular matrix were discernable (Figure 2b). An explanation for this lack of structure is given by the opposite effects of the viscosity[42] and of the refractive index n ($\tau_F = C/n^2$)[43] on the fluorescence lifetime of DASPI. The intercellular matrix is more viscous than the cytosol inside the cells, so that the fluorescence lifetime of

Table 1. Comparison of the fluorescence lifetimes [ps] measured in monoexponential and biexponential FLIM.

	Homogenous medium				Heterogeneous medium	
	DBT 22 (ethanol)	Rh B (ethanol)	β-NADPH (dist. aq.)	Rh B (dist. aq.)	DASPI (ASC)	Rh B (ASC)
monoexp. FLIM	495	2587	412	1530	61	1530
biexp. FLIM	472	2608	399	1504	68	1377[a]
					1468[b]	1502[c]

[a] Fluorescence lifetime of rhodamine B averaged over the whole τ map, uncorrected for the refractive index n. [b] Fluorescence lifetime of rhodamine B in the intercellular matrix averaged over seven regions, corrected for n. [c] Fluorescence lifetime of rhodamine B in the cell interior averaged over six cells, corrected for n.

DASPI in the intercellular regions should be significantly larger.[42] However, a larger refractive index of the intercellular matrix ($n = 1.43$) than of the cell interior ($n = 1.34$) leads to a reduction of τ_F in the intercellular regions and, thus, to a homogenisation of the fluorescence lifetime all over the image. The refractive index of the artificial epidermis has been determined by means of monoexponential FLIM in ASC stained with coumarin 314 (data not shown). Since the fluorescence lifetime of coumarin 314 is not influenced by pH, viscosity or ion concentration, this dye is adequate as an indicator of the refractive index (data not shown).

The τ_2 map of rhodamine B (Figure 2 c) shows clear differences between the cell interior and the intercellular matrix. The fluorescence lifetime inside the cells (1480 ± 50 ps averaged over six cells) is larger than that in the intercellular matrix (1270 ± 70 ps averaged over seven regions) because the refractive index of the lipidlike membranes ($n = 1.43$) is considerably larger than that of the cytosol ($n = 1.34$). The values of the fluorescence lifetime of rhodamine B corrected for the refractive index are 1468 ± 83 ps in the intercellular regions and 1502 ± 51 ps in the cytosol. Thus, both in the cell interior and in the intercellular matrix, the fluorescence lifetime of rhodamine B corrected for n corresponds within error margins to the lifetime measured in water. The effect of viscosity on the fluorescence lifetime of rhodamine B is negligible (data not shown).

The contribution $\tau_2 a_2/(\tau_1 \cdot a_1 + \tau_2 \cdot a_2)$ of rhodamine B to the cumulative fluorescence signal amounts to 98%, while the remaining 2% represents the DASPI contribution. The ratio map, which shows a spatial distribution of $\tau_2 a_2/(\tau_1 \cdot a_1 + \tau_2 \cdot a_2)$, does not reveal any differences between cell interior and intercellular matrix.

The experimental conditions were a scanned surface of 36×45 μm², a laser energy of 0.015 pJ pixel⁻¹, an excitation wavelength of 830 nm and an acquisition time of 9 s per image. Under these conditions, the sample did not suffer any photodamage. The contribution of cell-autofluorescence to the fluorescence signal was less than 0.05%. In the FLIM experiments, we recorded 51 images at different delays in 100 ps steps.

The good separation of DASPI and rhodamine B in the artificial skin constructs shows that, even in highly scattering media—which implies a high experimental noise—our analysis provides an accurate evaluation of multiexponential FLIM.

3.2. Endogenous NAD(P)H Fluorescence of Human Dermal Fibroblasts in ASC

We intend to demonstrate the applicability of biexponential FLIM combined with the Prony method in the investigation of the metabolic state of human dermal fibroblasts in artificial skin constructs by means of NAD(P)H endogenous fluorescence.

The fluorescence of an artificial dermis, 40–100 μm in depth, after illumination at 765 nm was observed. Under these conditions, only the fibroblasts show endogenous fluorescence. The collagen matrix and the growing medium do not fluoresce, as verified by autofluorescence experiments of a pure collagen solution and the growing medium. The scanned regions were 50×50 μm² and the laser energy E_{pix} was varied between 0.015 and 0.15 pJ pixel⁻¹.

It was shown that, at an excitation wavelength of ≈ 750 nm, the main contributors to the cellular endogenous fluorescence are the coenzymes NAD(P)H: free or involved in metabolic processes.[1,2,7,8,10,11] The assumption that the intrinsic fluorescence of the fibroblasts observed at $\lambda = 765$ nm originates from NAD(P)H is supported by the fact that the exposure of the skin to equivalents of sodium cyanide resulted in an increase in the fluorescence signal of up to 200%.[8] Moreover, the fluorescence in the cells stems from small granules in the cytosol, mostly organised around the nonfluorescing cell nucleus (Figure 3). These granules are primarily ascribed to mitochondria, that is, organelles with a high content of NAD(P)H due to their metabolic function.[10]
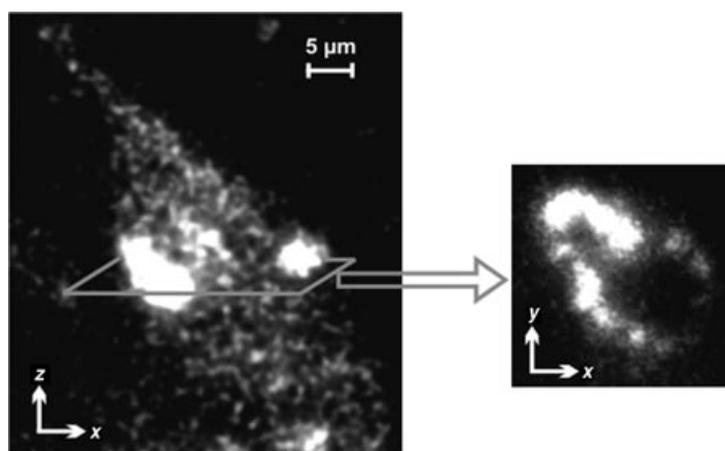

Figure 3. Autofluorescence images of dermal fibroblasts in ASC, longitudinal (left) and transverse (right) optical sections. The organelle around the nonfluorescing nucleus, the mitochondria, are the brightest due to their high NAD(P)H content. Employed experimental parameters: $\lambda = 765$ nm, $E_{pix} = 0.039$ pJ pixel⁻¹, depth = 60 μm.

The steady state fluorescence images (Figures 3 and 4a) mirror the distribution of the cumulative concentration of both free and protein-bound NAD(P)H, but do not give any information about the ratio between their concentrations and, thus, about the cellular metabolic state. Since the fluorescence lifetime of the free (≈ 400 ps) and protein-bound (≈ 2000 ps) NAD(P)H differ significantly,[10] the biexponential FLIM combined with the Prony method is optimal for rapidly obtaining this information, which is contained in the cumulative NAD(P)H fluorescence signal. Moreover, the biexponential approximation is in this case the appropriate approach, due to the fact that the cumulative NAD(P)H fluorescence decay deviates considerably from monoexponential behaviour (data not shown).
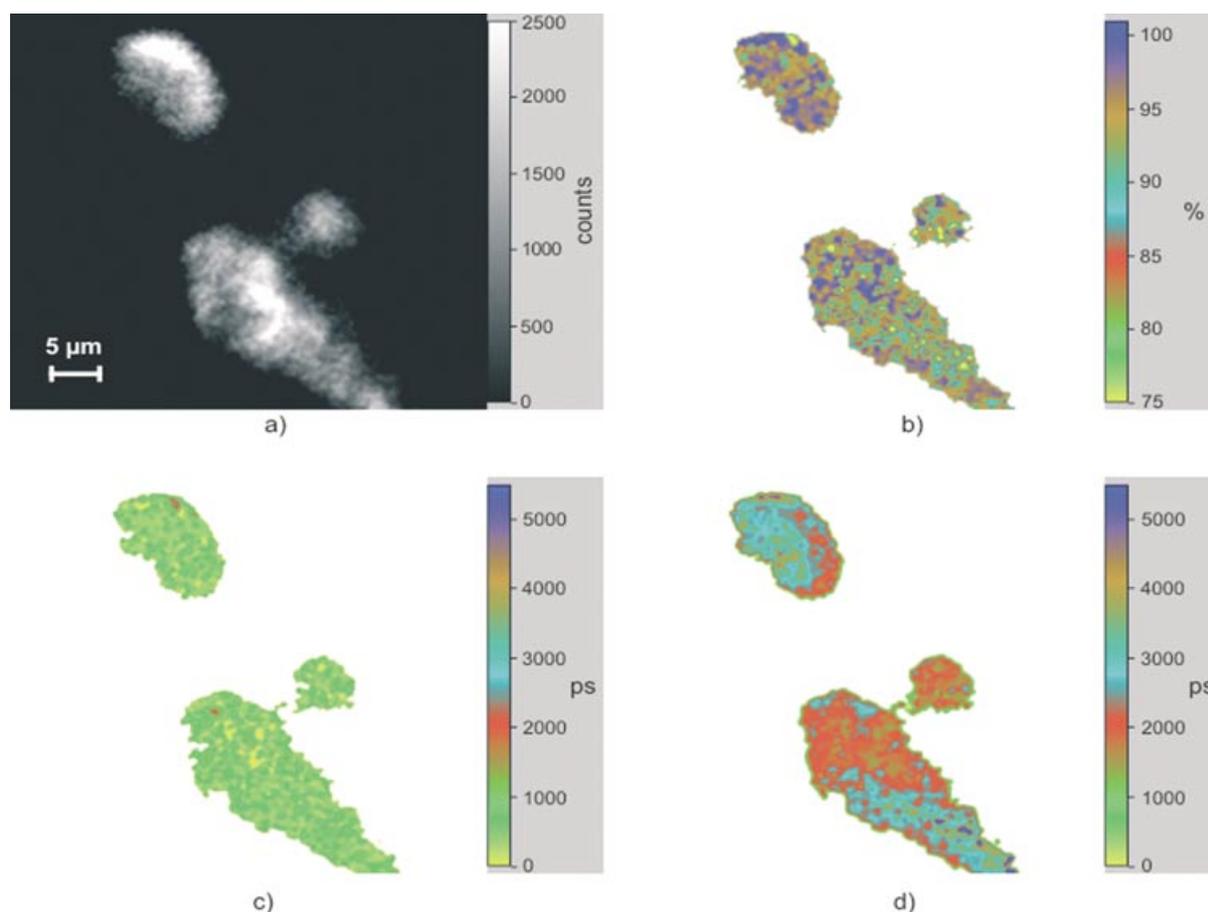
Figure 4. *Free and protein-bound NAD(P)H autofluorescence in three fibroblasts 73 μm in depth: a) steady state intensity image, b) ratio map, that is, the contribution of the protein-bound NAD(P)H to the cumulative fluorescence signal, c) τ_1 map corresponding to the free NAD(P)H, d) τ_2 map corresponding to the NAD(P)H involved in metabolic processes. $E_{pix}=0.055$ pJ pixel^{-1}.*

In monoexponential FLIM experiments, we determined the fluorescence lifetime of the free NADH and NADPH to be 444 ± 16 ps and 412 ± 15 ps, respectively. These values agree with results published by others.[10]

A typical result of a biexponential FLIM experiment includes a τ_1 map attributed to the free NAD(P)H (Figure 4c), a τ_2 map attributed to the NAD(P)H involved in metabolic processes (Figure 4d) and an image which mirrors the contribution $\tau_2 a_2/(\tau_2 a_2+\tau_1 a_1)$ of the protein-bound NAD(P)H to the cumulative fluorescence signal (Figure 4b).

The average fluorescence lifetime in a τ_1 map amounts to 430 ± 20 ps (averaged over 12 τ_1 maps) and corresponds (within error margins) to the fluorescence lifetimes of the free NADH and free NADPH measured in monoexponential FLIM experiments. Consequently, the correctness of the performed experiments is illustrated. Since free NADH and NADPH cannot be resolved in FLIM experiments, the resulting fluorescence lifetime of NAD(P)H, that is, a weighted average of the lifetimes of NADH and NADPH, differs slightly from the values measured for the pure components. Further deviations of the lifetime τ_1 from the fluorescence lifetimes of the pure NADH and NADPH, respectively, are attributed to different environmental parameters, for example, viscosity, refractive index or pH, in the mono- and biexponential FLIM experiments. The presence of two species (free NADH and free NADPH) and the effect of the environmental parameters in the cell interior are mirrored in the histogram shown in Figure 5, which displays the relative occurrence of the lifetimes τ_1. Since the FWHM (150 ± 50 ps) of this distribution is comparable to the width of distributions determined in biexponential FLIM experiments in homogenous media, the effect of the factors mentioned above is of minor importance.

The average of the fluorescence lifetimes of the protein-bound NAD(P)H in a τ_2 map amounts to ≈ 2000 ps (2250 ± 200 ps averaged over 12 τ_2 maps), as expected.[10]. However, the protein–NAD(P)H complexes characterised by different fluorescence lifetimes (between 1000 and 4000 ps) are not uniformly distributed all over the cell interior as has previously been assumed, but, rather, they are concentrated in certain cellular regions (Figure 4d). Consequently, we have demonstrated that by employing biexponential FLIM it will be possible to monitor different metabolic processes simultaneously in different regions of the cell and, thus, to get a deeper insight into the mechanisms of cellular metabolism. The large variety of binding possibilities of NAD(P)H as a cofactor is also mirrored in the width (1050 ± 100 ps) of the histogram (Figure 5), which shows the relative occurrence of the lifetimes τ_2.
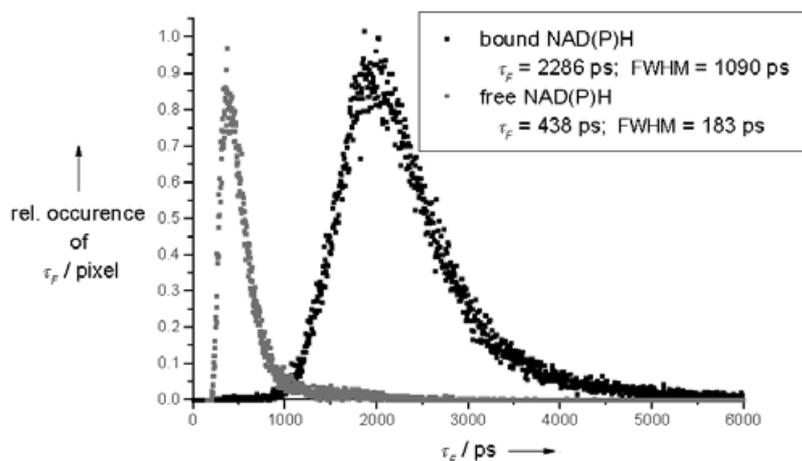
Figure 5. *Relative occurrence of the fluorescence lifetimes of free and protein-bound NAD(P)H in the fibroblasts pictured in Figure 4.*

The ratio maps, which show the relation between the contents of the free and protein-bound NAD(P)H, provide the most important information, that is, the cellular metabolic activity in each pixel of the image at a certain point in time. Variations of the ratio $\tau_2 a_2/(\tau_2 a_2 + \tau_1 a_1)$ within the cell indicate slower and faster metabolic activities in different organelles. For instance, in Figure 4b, small granules with a high content ($\approx 100\%$) of protein-bound NAD(P)H—which are characterised by a high metabolic activity—are surrounded by the cytosol characterised by a lower $\tau_2 a_2/(\tau_2 a_2 + \tau_1 a_1)$ ratio.

In order to demonstrate the applicability of the presented biexponential FLIM technique in monitoring the cellular metabolic activity under the influence of external factors, we performed FLIM experiments on fibroblasts in ASC under NIR photostress at seven different energies E_{pix} (0.015, 0.02, 0.039, 0.055, 0.078, 0.118, 0.152 pJ pixel^{-1}). In this way, the dependence of the cellular reaction on the illumination energy indicated by the metabolic state could be easily quantified (Figure 6). As anticipated by König et al.,[10] the contribution of the protein-bound NAD(P)H to the cumulative autofluorescence signal
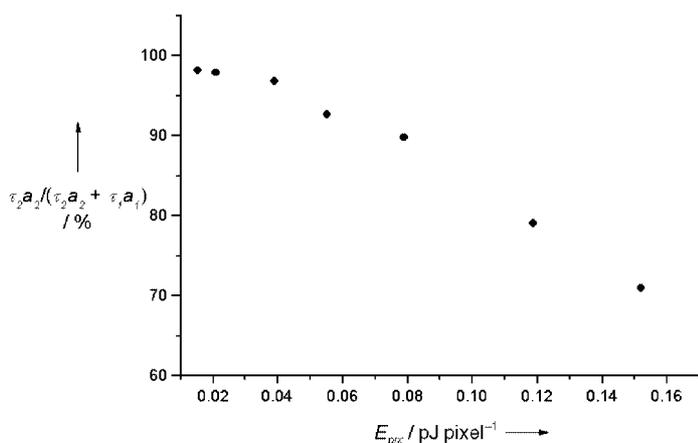
and, consequently, also the relative concentration of the protein-bound NAD(P)H decreases with increasing laser energy E_{pix} and, thus, the metabolic activity is slower for a more intense NIR photostress.

Whereas at low laser energies (E_{pix}) the cell merely exhibits a slower metabolism, at higher energies morphological changes, plasma formation and finally intracellular optical breakdown occur.[7] In our experiments, such phenomena occurred only after an exposure time of ≈ 1 h and at laser energies larger than 0.285 pJ pixel^{-1}.

For the FLIM experiments, we registered 15 to 20 intensity images at consecutive delays in 200 ps steps. The exposure time was 11 s per image.

4. Summary

We implemented for the first time in FLIM a noniterative evaluation method generally applicable for multiexponential approximations. We verified its accuracy by comparing the fluorescence lifetimes obtained in biexponential FLIM experiments in both homogenous and heterogeneous media with those determined in monoexponential FLIM experiments. To probe the limits of the evaluation method, extreme parameters were selected for these experiments: large intensity ratios $\tau_2 a_2/\tau_1 a_1$, that is, the signal of one component was almost masked by the background, and relatively low lifetime ratios τ_2/τ_1 (3.7) for which a separation of the fluorescence lifetimes of the components is difficult. The fluorescence lifetimes determined in biexponential FLIM experiments deviated from those determined in monoexponential FLIM experiments by less than 5%.

The rapidity and high accuracy of our method will allow dynamical two- and three-dimensional-multiexponential FLIM in real time to be performed.

We also demonstrated the applicability of biexponential FLIM combined with the presented noniterative evaluation technique in the investigation of the cellular metabolism of dermal fibroblasts from ASC by means of endogenous NAD(P)H fluorescence. Thereby, we showed for that the protein–NAD(P)H complexes involved in metabolic processes are not uniformly distributed all over the cell, but are concentrated in certain cellular regions. By employing the presented method, changes in the metabolic activity of the dermal fibroblasts could be directly visualised in the ratio maps, as we verified in experiments in which the metabolic activity of the cells under NIR photostress was probed.

Figure 6. *Dependence of the ratio $\tau_2 a_2/(\tau_2 a_2 + \tau_1 a_1)$, the contribution of the protein-bound NAD(P)H to the cumulative autofluorescence signal, on the laser energy E_{pix}.*

Experimental Section

The basic set-up of the two-photon microscope used in our experiments is similar to that described by König et al.[10] The characteristics of the pulsed laser beam of the Ti:Sa-laser (Mira 900, Coherent) are: a 200-fs pulse width, 76-MHz repetition rate and 169-nJ pulse energy. The laser beam was driven by two galvanometric mirrors (GSI Lumonics) in order to scan the sample in the *x–y* plane perpendicular to the optical axis. In the *z* direction (on the optical axis) the sample was driven by a piezoelectric stage (Physics Instruments) with a precision of 8.42 nm. A microscope objective Achroplan (63×, NA = 0.95, water-immersion, Carl Zeiss) was used to focus the tenfold extended laser beam into the sample. The dimensions of the effective two-photon excitation volume were for a wavelength λ of 800 nm $\omega_0 = 0.42$ µm in the *x–y* plane and $z_e = 1.35$ µm on the optical axis. The calibration was performed by means of fluorescent latex microbeads for the *x--y* resolution and of fluorescein–isothiocyanide-monolayers for the *z* resolution.[25] As the detection unit in the FLIM experiments, we used a time-gated system (LaVision) including a high repetition rate intensifier (HRI) with an adjustable gate (200–1000 ps) combined with a water-cooled CCD camera (480×640 pixels). The jitter of the detection system was less than 10 ps (8–9 ps measured in almost noise-free FLIM experiments) at a gate width of 200 ps. A pixel on the CCD chip corresponds to 0.145 ± 0.05 µm at the sample. The dwell time of the laser beam per pixel during one scan was 0.95 µs. The excitation energy per pixel, E_{pix}, during one scan was varied between 0.015 and 0.285 pJ pixel⁻¹. The size of the scanned field was varied between 25×25 and 50×50 µm². 15 to 51 fluorescence intensity images were registered at subsequent delays after the pulse in steps of 100 or 200 ps, to generate the τ images.

In the FLIM experiments, we used Rhodamine B, β-NADPH, β-NADH, DASPI (Fluka, Germany), DBT 22 (synthesised by Kroener, TU Braunschweig), ethanol and DMSO p.a. without further purification.

The artificial skin constructs (ASC) were kindly provided by Prof. Dr. C. C. Mueller-Goymann, TU Braunschweig. The ASC consisted of a collagen matrix with incorporated human dermal fibroblasts (HDF), the dermis equivalent, covered by an epidermis equivalent of HaCaT (human adult at low calcium concentration and elevated temperature) keratinocytes.[44] The autofluorescence experiments were performed 1–2 h after the constructs were removed from the incubator. For the labelling experiments, the ASC were stained with an aqueous mixture (pH 7.15) of DASPI (83 µM) and rhodamine B (17 µM). For this, 2 mL of this solution was mixed in the growing medium of the skin constructs. To achieve a rapid staining, 5 µL of DMSO was also added. The experiments were performed within 2 h of removing the samples from the incubator. During this period, a sufficient concentration of the chromophores was assimilated by the samples.

Acknowledgements

[1] B. R. Masters, P. T. C. So, E. Gratton, *Biophys. J.* **1997**, *72*, 2405–2412.
[2] D. W. Piston, B. R. Masters, W. W. Webb, *J. Microscopy* **1995**, *178*, 20–27.
[3] K. König, U. Wollina, I. Riemann, C. Peuckert, K.-J. Halbhuber, H. Konrad, P. Fischer, V. Fünfstück, T. W. Fischer, P. Elsner, *Proc. SPIE* **2002**, *4620*, 191–201.
[4] G. H. Patterson, S. M. Knobel, P. Arkhammar, O. Thastrup, D. W. Piston, *Proc. Natl. Acad. Sci. USA* **2000**, *97*, 5203–5207.
[5] D. W. Piston, S. M. Knobel, *Trends Endocrinol. Metab.* **1999**, *10*, 413–416.
[6] S. Maiti, J. B. Shear, R. M. Williams, W. R. Zipfel, W. W. Webb, *Science* **1997**, *275*, 530–532.
[7] K. König, *J. Microscopy* **2000**, *200*, 83–104.
[8] S. Huang, A. A. Heikal, W. W. Webb, *Biophys. J.* **2002**, *82*, 2811–2825.
[9] Q. Zhang, D. W. Piston, R. H. Goodman, *Science* **2002**, *295*, 1895–1898.
[10] K. König, P. T. C. So, W. W. Mantulin, B. J. Tromberg, E. Gratton, *J. Micro.* **1996**, *183*, 197–204.
[11] K. König, P. T. C. So, W. W. Mantulin, E. Gratton, *Opt. Lett.* **1997**, *22*, 135–136.
[12] W. Denk, J. H. Strickler, W. W. Webb, *Science* **1990**, *248*, 73–76.
[13] W. Becker, A. Bergmann, www.becker.de/pdf/tcvgbh1.pdf, Feb. **2003**.
[14] J. R. Lakowicz, K. Berndt, *Rev. Sci. Instrum.* **1991**, *62*, 1727–1734.
[15] J. Pawley, *Handbook of Biological Confocal Microscopy*, Plenum Press, New York, **1995**, pp. 491–505.
[16] K. M. Hanson, M. J. Behne, N. P. Barry, T. M. Mauro, E. Gratton, R. M. Clegg, *Biophys. J.* **2002**, *83*, 1682–1690.
[17] J. R. Lakowicz, H. Szmacinski, M. L. Johnson, *J. Fluorescence* **1992**, *2*, 47–62.
[18] J. Digel, T. Kobayashi, Z. Gryczynski, J. R. Lakowicz, J. H. Collins, *Arch. Biochem. Biophys.* **2001**, *387*, 243–249.
[19] H. Szmacinski, J. R. Lakowicz, *Anal. Biochem.* **1997**, *250*, 131–138.
[20] H. C. Gerritsen, R. Sanders, A. Draaijer, Y. K. Levine, *J. Fluorescence* **1997**, *7*, 11–16.
[21] S. Murata, P. Herman, J. R. Lakowicz, *Cytometry* **2001**, *43*, 94–100.
[22] W. Becker, A. Bergmann, C. Biskup, T. Zimmer, N. Klöcker, K. Benndorf, *Proc. SPIE* **2002**, *4620*, 79–84.
[23] A. Squire, P. J. Verveer, P. I. H. Bastiaens, *J. Microscopy* **2000**, *197*, 136–149.
[24] P. J. Verveer, A. Squire, P. I. H. Bastiaens, *Biophys. J.* **2000**, *78*, 2127–2137.
[25] A. Schönle, M. Glatz, S. W. Hell, *Appl. Opt.* **2000**, *39*, 6306–6311.
[26] V. Barzda, C. J. Grauw, J. Vroom, F. J. Kleima, R. van Grondelle, H. van Amerongen, H. C. Gerritsen, *Biophys. J.* **2001**, *81*, 538–546.
[27] P. T. C. So, H. Kim, *Opt. Exp.* **1998**, *3*, 339–350.
[28] B. R. Masters, P. T. C. So, E. Gratton, *Ann. N.Y. Acad. Sci.* **1998**, *838*, 58–67.
[29] K. C. Benny Lee, J. Siegel, S. E. D. Webb, S. Lévêque-Fort, M. J. Cole, R. Jones, K. Dowling, M. J. Lever, P. M. W. French, *Biophys. J.* **2001**, *81*, 1265–1274.
[30] E. Gratton, S. Breusegem, J. Sutin, Q. Ruan, N. Barry, *J. Biomed. Opt.* **2003**, *8*, 381–390.
[31] P. J. Verveer, P. I. H. Bastiaens, *J. Microscopy* **2003**, *209*, 1–7.
[32] A. D. Scully, R. B. Ostler, D. Phillips, P. O'Neill, K. M. S. Townsend, A. W. Parker, A. J. MacRobert, *Bioimaging* **1997**, *5*, 9–18.
[33] R. J. Woods, S. Scypinski, L. J. Cline Love, H. Ashworth, *Anal. Chem.* **1984**, *56*, 1395–1400.
[34] R. M. Ballew, J. N. Demas, *Anal. Chem.* **1989**, *61*, 30–33.
[35] K. K. Sharman, A. Periasamy, H. Ashworth, J. N. Demas, N. H. Snow, *Anal. Chem.* **1999**, *71*, 947–952.
[36] C. Stehning, G. Holst, *Proc. SPIE* **2001**, *4578*, 259–270.
[37] C.-E. Fröberg, *Numerical Mathematics—Theory and Computer Applications*, The Benjamin/Cummings Publishing Company, Inc., Menlo Park, California, **1985**, pp. 257–258.
[38] Z. Y. Zhang, T. Sun, K. T. V. Grattan, A. W. Palmer, *Proc. SPIE* **1997**, *2980*, 90–95.
[39] V. V. Apanasovich, E. G. Novikov, *Opt. Comm.* **1990**, *78*, 279–282.
[40] K. Sasaki, H. Masuhara, *Appl. Opt.* **1991**, *30*, 977–980.
[41] J. Enderlein, R. Erdmann, *Opt. Comm.* **1997**, *134*, 371–378.
[42] D. S. Elson, J. Siegel, S. E. D. Webb, S. Lévêque-Fort, M. J. Lever, P. M. W. French, K. Lauritsen, M. Wahl, R. Erdmann, *Opt. Lett.* **2002**, *27*, 1409–1411.
[43] S. J. Strickler, R. A. Berg, *J. Chem. Phys.* **1962**, *37*, 814–822.
[44] A. Winkler, C. C. Müller-Goymann, *Eur. J. Pharm. Biopharm.* **2002**, *53*, 281–287.